

Deep Contextual Clinical Prediction with Reverse Distillation

Rohan S. Kodialam
 CSAIL & IMES
 MIT
 Cambridge, MA
 kodialam@alum.mit.edu

Rebecca Boiarsky
 CSAIL & IMES
 MIT
 Cambridge, MA
 rboiar@mit.edu

David Sontag
 CSAIL & IMES
 MIT
 Cambridge, MA
 dsontag@csail.mit.edu

Abstract

Healthcare providers are increasingly using learned methods to predict and understand long-term patient outcomes in order to make meaningful interventions. However, despite innovations in this area, deep learning models often struggle to match performance of shallow linear models in predicting these outcomes, making it difficult to leverage such techniques in practice. In this work, motivated by the task of clinical prediction from insurance claims, we present a new technique called *reverse distillation* which pretrains deep models by using high-performing linear models for initialization. We make use of the longitudinal structure of insurance claims datasets to develop Self Attention with Reverse Distillation, or SARD, an architecture that utilizes a combination of contextual embedding, temporal embedding and self-attention mechanisms and most critically is trained via reverse distillation. SARD outperforms state-of-the-art methods on multiple clinical prediction outcomes, with ablation studies revealing that reverse distillation is a primary driver of these improvements.

1 Introduction

Clinical predictions using electronic health records (EHRs) are critical in providing preventative, prophylactic and palliative care. Deep learning techniques offer a path to improving predictive performance for such tasks by learning representations of longitudinal health records that capture a patient’s medical status and potential future risks. State-of-the-art models in the literature have largely focused on shorter-term prediction over horizons of days or weeks, most notably during a single hospital visit [1, 2, 3, 4, 5], or in the immediate aftermath of a visit [3, 4]. Approaches to longer-term prediction often rely on manually feature-engineering longitudinal health data into patient state vectors [6, 1, 7, 8], as opposed to training end-to-end from raw longitudinal EHR data. Due to this heuristic approach, these methods cannot fully exploit the temporal nature of EHR data, nor the relationships between clinical concepts. We further find that linear models with well-tuned features are quite competitive with existing end-to-end deep models for long-term prediction, indicating that deep learning successes in other domains have not yet been effectively translated to clinical prediction [9, Supplemental Table 1].

This paper contributes Self Attention with Reverse Distillation, or SARD, a self-attention based architecture for longitudinal health data; and reverse distillation, a novel training procedure to initialize deep models using strong baselines. SARD uses a combination of a Deep Set transformation [10] to efficiently embed very sparse data, followed by a self-attention mechanism [2] to extract meaning from the temporal structure of medical claims and the relationships between clinical concepts. We train SARD using reverse distillation, in which we first initialize our model to mimic a performant linear model, and subsequently fine-tune.

We find empirical evidence that reverse distillation acts as an effective way to perform soft feature selection over complex feature spaces, such as multidimensional time-series data. We further establish statistically significant gains in terms of predictive performance on three tasks – predicting the likelihood of a patient dying, requiring surgery, and requiring hospitalization – with clear applications to preventative and palliative healthcare. Our experiments also establish that reverse distillation is a key driver behind these wins, and pave the way for the use of this method in future research.

2 Background

EHRs represent collections of longitudinal patient-level medical encounter data. In our work, we focus on a subset of structured EHR data, medical claims, that are frequently found in health insurance databases. For each patient, we receive a time series of *visits* – single continuous interactions of a patient with the healthcare system – and *codes* – the medical events occurring during each visit. These codes detail the specialties of visited doctors, diagnoses, procedures, the administration of drugs, and other medical concepts.

Machine learning models operating on claims data must learn from their rich temporal and conceptual structure to create a patient-level representations. The following key properties of claims data inform our architectural choices:

Sparsity of Features: Claims data is extremely sparse. The set of codes is large, and the overwhelming majority of codes do not apply to a given patient at a given time. For example, if our data were fully expanded as a dense matrix, only 1 in 10^6 elements would be nonzero. It is therefore important for architectures to account for this sparsity – in several prior works, this is achieved by storing data as sparse multi-hot vectors representing active codes [11, 12].

Visit-level Temporality: Visits are ordered and augmented with timestamps corresponding to when care was provided. The architecture must process a highly irregularly-spaced time series of events, since care is often administered in short bursts punctuated by long gaps. Highly variable timescales must be simultaneously accounted for, since the time between visits made by a single patient can vary from years to days. This has been previously approached by discretizing time to allow for uniform time steps [13], bucketizing time [6] to create categorical representations, or treating time as a continuous covariate in models [14, 5].

Long-Term Dependencies: Visits occur for a multitude of reasons, and a simple temporal ordering of visits cannot capture the multiple parallel narratives formed by visits. Noting that the time between events in each narrative can vary, the model must be able to efficiently capture variable-term dependencies. We discuss several prior approaches, including recurrent and convolutional strategies, to address this challenge below.

Many recent works analyze how deep learning can be applied to clinical prediction [11, 9, 15, 16, 12, 17, 18, 19, 20]. Several approaches use recurrent neural networks (RNNs) to ingest medical records, and achieve excellent performance on tasks like predicting in-patient mortality upon hospital admission [11]. Further refinements add learned imputation to account for missingness [15], and improvements in featurizing time by using architectures like bi-directional RNNs [21] and two-level attention mechanisms to find the influence of past visits on a prediction [12, 14]. Research has also focused on using convolutional neural networks (CNNs) to develop better embeddings of clinical concepts passed into a recurrent model [19], and graphically representing the patient-clinician relationship to augment health record data [20]. Self-attention has also been used in a non-longitudinal manner, to develop relationships between medical features that have already been collapsed over the temporal dimension using recurrent methods [22].

When making predictions with horizons of months or years, the state-of-the-art is still simple, often linear models with carefully chosen features [6, 1]. Recent work exploring deep-learning based approaches to long-term clinical prediction train neural networks directly on features constructed using hand-picked time windows and summary statistics [7] or use denoising autoencoders to pre-process this type of data [8], and do not necessarily beat linear baselines [9, Supplemental Table 1]. Critically, many of these models rely on manual feature-engineering to create representations of the time-series data that forms a patient’s medical record rather than learning this structure in tandem with the task at hand.

3 Representing Longitudinal Health Data with Self-Attention

Our proposed architecture addresses the challenges described in Section 2 by building upon self-attention architectures [2], which have seen success in natural language processing [23] and time-series analysis [24, 25]. Self-attention mechanisms allow each element of a sequence to extract context from, or *attend* to, other sequence elements. What makes this paradigm particularly appealing is that any element can directly attend to any other element regardless of their separation within the sequence, which means that long-term dependencies are captured well. This is in contrast to recurrent or convolutional methods, where information must flow through many layers of computation to get from one sequence element to a distant other. Using self-attention, SARD is able to cleanly and interpretably associate visits over a variety of timescales.

We use a set encoding approach to address the challenge of sparsity and the need to represent a set of data observed at each visit, and a self-attention based architecture to allow any visit’s embedding to interact with another visit embedding through $O(1)$ layers, thus ensuring that we can capture temporal information and dependencies. An overview of the architecture is provided in Figure 1.

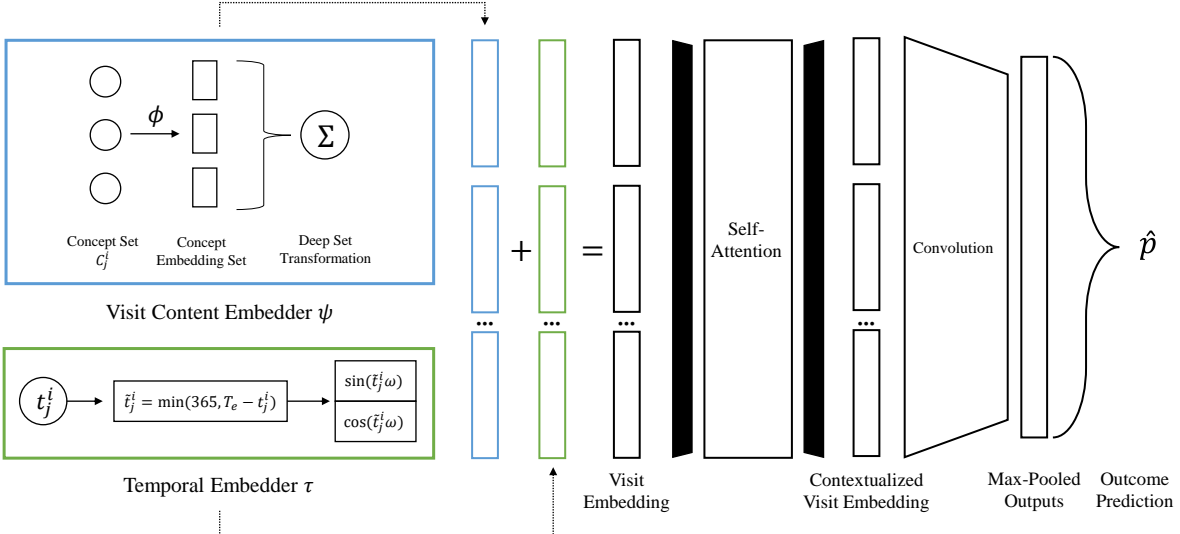


Figure 1: SARD Architecture for Longitudinal Claims Data

We denote the set of visits made by a patient i by \mathcal{V}_i , and represent this patient’s j th visit by V_j^i . We further denote the time of visit V_j^i by t_j^i and the set of codes assigned during visit V_j^i with $C_j^i \subseteq \mathcal{C}$.

Input Embedding: We adapt the method of Choi et al. [26] to generate an initial concept embedding map $\phi : \mathcal{C} \rightarrow \mathbb{R}^{d_e}$, learned only using data in the training window to prevent label leakage. The vector representation $\psi(V_j^i) \in \mathbb{R}^{d_e}$ of each visit is calculated as $\psi(V_j^i) = \sum_{c \in C_j^i} \phi(c)$, providing invariance to permutations of the codes. This is similar to the Deep Sets paradigm, with nonlinearity provided by the embedding ϕ and downstream components of our architecture [10].

Temporal Embedding: SARD does not explicitly encode the order of events, and visits do not occur in regular intervals. We embed the time of each visit into \mathbb{R}^{d_e} using sinusoidal embeddings [2], and generate a *temporal embedding* $\tau(V_j^i) = \sin(\tilde{t}_j^i \omega) \parallel \cos(\tilde{t}_j^i \omega)$, where $\tilde{t}_j^i = \min(365, T_A - t_j^i)$ and T_A represents the prediction date. This allows us to measure time relative to the prediction date. Note that we denote concatenation with \parallel , ω is a length $d_e/2$ vector of frequencies in geometric progression from 10^{-5} to 1, and sin and cos are applied element-wise.

Self-Attention: We add $\psi(V_j^i)$ and $\tau(V_j^i)$ to create final encodings that represent the content and timing of visits. To contextualize visits in a patient’s overall history we use multi-headed self-attention [2] with $L = 2$ self-attention blocks and $H = 2$ heads. For efficiency, we truncate to the $n_v = 512$ most recent visits, and add padding for patients with less than n_v visits, but use a masking mechanism to only allow non-pad visits to attend to each other. We apply dropout with probability $\rho_d^t = 0.3$ after each self-attention block to prevent overfitting. This approach allows any visit to attend to any other, so longer-range dependencies of clinical interest can be learned.

Each layer of each head performs three affine transformations on the input embeddings, which for the first layer are $\psi(V_j^i) + \tau(V_j^i)$ for each visit V_j^i . These transformations produce vectors k_j^i, q_j^i and v_j^i respectively. We find the contextualized embedding of visit V_j^i by computing raw attention weights $w_{j\ell}^i = q_j^i \cdot k_\ell^i / \sqrt{d_e}$, normalizing via softmax to $\tilde{w}_{j\ell}^i = \left(\sum_{\ell=1}^{n_v} e^{w_{j\ell}^i} \right)^{-1} e^{w_{j\ell}^i}$, and taking the weighted sum $\sum_{\ell=1}^{n_v} \tilde{w}_{j\ell}^i v_\ell^i$. This process is then repeated at each layer using the contextualized embeddings as inputs, and residual connections are used between layers. The outputs of each head are concatenated to create final, contextualized visit representations $\tilde{\psi}(V_j^i)$.

Convolutional Prediction Head: The prediction head returns an estimated probability of the target event using the outputs of the self-attention mechanism. We do so by creating K convolutional kernels of size $d_e \times 1$. Then, each kernel extracts a feature from the non-pad contextualized visit embeddings by first calculating a cross-correlation versus each $\tilde{\psi}(V_j^i)$, then using a max-pooling operation to select the highest of these cross-correlations. Concatenating these outputs gives a length- K real vector of extracted features. To obtain a predicted probability $\hat{p}(i)$ for each patient, we apply a sigmoid nonlinearity to this vector, take the dot product of the transformed components with a learned vector of weights, and apply another sigmoid nonlinearity to obtain a final prediction probability.

4 Learning with Reverse Distillation

Reverse distillation is a novel method by which we initialize a deep model using a linear proxy. We consider a binary prediction model $f_\theta : \mathcal{X} \rightarrow [0, 1]$ parametrized by θ which maps from a domain \mathcal{X} of data to a probability value, and a linear model $g_w : \mathcal{X} \rightarrow [0, 1]$ defined by $g_w(x) = \sigma(w^T \xi(x))$, where σ is the sigmoid function and ξ is a fixed *feature engineering* transformation $\xi : \mathcal{X} \rightarrow \mathbb{R}^d$ based on heuristic domain knowledge.

While f_θ may be a large, highly-parametrized model, g_w may perform better on prediction tasks for several reasons, including the ability to select features and avoid overfitting through regularization of w , and the quality of the transformation ξ . As such, we initialize f_θ to mimic the outputs of g_w in order to benefit from the structure and performance of the linear model while allowing for further data-driven improvements.

We interpret predictions $f_\theta(x)$ (resp $g_w(x)$) as indicating that the distribution of the label for data point x is $\mathbf{B}(f_\theta(x))$ (resp $\mathbf{B}(g_w(x))$), where $\mathbf{B}(p)$ indicates a Bernoulli distribution with success parameter p . We perform reverse distillation by training our deep model by optimizing over θ a loss function defined by

$$\ell_{\text{RD}}(x) = D_{\text{KL}}(\mathbf{B}(g_w(x)) \parallel \mathbf{B}(f_\theta(x))). \quad (1)$$

This algorithm is inspired by the standard knowledge distillation paradigm [27], in which a simpler model is trained to mimic a complex model. To fine-tune f_θ , we make use of both the true label $y(x) \in \{0, 1\}$ and the prediction $g_w(x)$, combining a cross-entropy loss versus the true label and the discrepancy between g_w and f_θ with a hyperparameter α to get a loss function

$$\ell_{\text{tune}}(x) = -y(x) \log f_\theta(x) \quad (2)$$

$$- (1 - y(x)) \log(1 - f_\theta(x)) \quad (3)$$

$$-\alpha g_w(x) \log f_\theta(x) \quad (4)$$

$$-\alpha(1 - g_w(x)) \log(1 - f_\theta(x)). \quad (5)$$

Note that the last two terms in ℓ_{tune} are equal to the KL divergence between $g_w(x)$ and $f_\theta(x)$ up to an additive constant, which we remove to allow α to solely represent the weight placed on differences between $g_w(x)$ and $f_\theta(x)$.

Training Procedure for SARD. We next describe our procedure for training a SARD model with reverse distillation. All training is performed end-to-end, including the initial embedding ϕ of clinical concepts. We reverse distill from a highly L_1 -regularized logistic regression model. As the logistic regression's predictions tend to be well-calibrated [3], we interpret its output as a distribution over outcomes. While hand-engineered features are often created for specific tasks in the clinical domain, we opt for a more general formulation. Inspired by prior work in high-performance linear models for clinical prediction [6], we construct features by aggregating codes over different temporal windows. Given a time interval $W = [t_s, t_e]$, we find the feature vector corresponding to this interval for patient i by finding the subset of visits $\mathcal{V}_i(W) = \{V_j^i \in \mathcal{V}_i \mid t_j^i \in W\}$ and subsequently finding the set of codes $\mathcal{C}_i(W) = \bigcup_{V_j^i \in \mathcal{V}_i(W)} \mathcal{C}_j^i$. We find that performance was optimized by using a multi-hot vector $f_i(W)$ of size $|\mathcal{C}|$ to represent these sets, with the element corresponding to concept $c \in \mathcal{C}$ set equal to 1 if $c \in \mathcal{C}_i(W)$ and 0 otherwise.

To capture the longitudinal nature of claims data, we use multiple windows simultaneously as features. We establish a list \mathcal{W}_C of candidate windows, each of which has an end time equal to the prediction date and start times ranging from 15 to ∞ days before the prediction date, as shown in Appendix Table 6. We selected the $n_W = 5$ best windows from all $\binom{|\mathcal{W}_C|}{n_W}$ unique window choices by comparing validation performances.

Theoretical analysis. We note that a deep model and a linear model making the same classifications are not necessarily learning the same classification boundary. We investigate if the self-attention model actually replicates the linear model's classification function.

We find that it is possible to construct a set of weights such that SARD and a windowed logistic regression model have identical outputs for all inputs:

Lemma 4.1. *In the limit $d_e \rightarrow \infty, K \rightarrow \infty$ and for an appropriate choice of ω , SARD can identically replicate a windowed linear model.*

The proof can be found in Appendix Section 8. The crux of the argument is that we can express a filter of the form $[[t_j^i < T]]$ for any T as a linear combination of the elements $\tau(V_j^i) = \sin(t_j^i \omega) \parallel \cos(t_j^i \omega)$, with weights determined as Fourier series coefficients. This allows SARD to replicate the windowed feature vectors of the linear model. We note that this lemma holds even with a single self-attention layer. This result increases our confidence in our choice of architecture and its ability to generalize and improve beyond a linear model. For example, windows of the form $[[t_j^i < T]]$ implied by the linear model might be inferior to a more complex filter in the time domain. However, such filters can be learned by SARD.

5 Experiments

We evaluate our approach using a de-identified dataset of 121,593 Medicare Advantage patients provided by Independence Blue Cross, a health insurance company with headquarters in Philadelphia. This data is mapped into the Observational Medical Outcomes Partnership (OMOP) common data model (CDM) version 6 [28]. OMOP provides a normalized concept vocabulary, and although our dataset is not public, hundreds of health institutions with data in an OMOP CDM can use our code out-of-the-box to reproduce results on local datasets¹. We also investigate the properties of reverse distillation through experimentation on synthetic data.

Baselines. We compare to four baselines. First, we compare against two logistic regression models: an L_2 -regularized model trained on a vector of counts of each code aggregated over a patient’s entire history, which was used as a baseline in prior work [12], and a time-windowed L_1 -regularized logistic regression model [6] trained as described in Section 4. Unlike [12], we normalize the count vectors in the L_2 -regularized model to sum to 1 instead of to have mean 0 and unit variance, so as to preserve sparsity structure. We also compare to our own self-attention-based model trained without reverse distillation, and RETAIN [12, 14], a deep learning model that previously achieved state-of-the-art performance on similar tasks. This baseline was chosen as it was developed for a dataset similar to ours, achieves good performance on long-term tasks, and offers an alternative way to use attention mechanisms to ingest longitudinal health data.

We train using a single NVIDIA k80 GPU. Our algorithms are implemented in Python 3.6 and use the PyTorch autograd library [29]. We train our deep models using an ADAM optimizer [30] with the hyperparameter settings of $\beta_1 = 0.9$, $\beta_2 = 0.98$, $\epsilon = 10^{-9}$ and a learning rate of $\eta = 2 \times 10^{-4}$. A batch size of 500 patients was used for ADAM updates.

Prediction tasks. We consider three tasks important for predictive healthcare:

- 1: The *End of Life (EoL)* prediction task: we estimate patient mortality over a six-month window. This task is key to proactively providing palliative care to patients.
- 2: The *Surgical Procedure (Surgery)* prediction task: we predict if a patient will require any surgical procedure in a six-month window. If so, an appropriate, intervention can be taken early on.
- 3: The *Likelihood of Hospitalization (LoH)* prediction task: we estimate if a patient will require inpatient hospitalization in a six-month window. This allows for early interventions that could mitigate the need for hospitalization.

We split the 121,593 patients into training, validation, and test sets of size 97,274, 5,000, and 19,319 respectively. Data was collected up to the end of the calendar year 2016, and outcomes measured between April and September of 2017. We denote the set of all OMOP concepts used in the dataset by \mathcal{C} , which in our case contained $|\mathcal{C}| = 37,004$ codes. All models are trained using the SARD architecture outlined in Section 3, using reverse distillation with early stopping for both pretraining and fine-tuning. SARD models are trained with $d_e = 300$, as we found that validation performance did not increase with larger embedding sizes. Early stopping and the selection of the hyperparameters as outlined in Appendix Table 6 are performed using the validation set, and the parameters that maximized validation ROC-AUC were used to evaluate performance on the test set. To assess the robustness of models under dataset shift, we additionally evaluated the performance of SARD and the windowed linear baseline at later time points in 2017 and 2018.

Our metric for measuring the performance is the area under the receiver-operator curve (ROC-AUC), i.e. the area under a plot of the true positive rate of the model as a function of false positive rate. An equivalent interpretation is the probability that the model gives a higher score to a random positive-outcome patient than a random negative-outcome patient. Thus, ROC-AUC is a good proxy for the application of choosing which patients should receive early interventions. This metric also is robust to class-imbalanced data, which is often the case in the clinical domain. Indeed, our class balances range from 1.8% for EoL up to 57.8% for Surgery.

5.1 Main results

As seen in Table 1, our model outperforms all baselines for each of the example tasks. Increases in AUC-ROC are significant versus the closest baseline in all cases (paired z -test, $p < .005$) [31]. In Section 5.2 we further explore the nuances of how SARD extracts clinical narratives, and qualitatively find that SARD is able to use a patient’s entire medical history to contextualize visits, whereas the high-performing linear models seem less able to make these connections.

Ablation Studies. We empirically test the design decisions made in Section 3 via ablation studies, details of which are given in Appendix Section 7. In addition to establishing the efficacy of reverse distillation, SARD’s temporal

¹Code provided on Github: <https://github.com/clinicalml/omop-learn>

Table 1: AUC-ROC Scores on Test Set. + RD indicates that reverse distillation is used for pretraining

Model \ Task Name	EoL	Surgery	LoH
Basic Linear Baseline [12]	76.3	69.9	65.4
RETAIN Recurrent Baseline [12]	82.3	80.5	72.3
Windowed Linear Baseline [6]	81.9	79.3	73.3
SARD (without RD)	84.4	82.9	73.1
SARD + RD	85.5	83.6	74.6

Table 2: AUC-ROC Scores for EoL on Test Sets using Jan 1, 2017 Model

Prediction Date	SARD + RD AUC	Windowed Linear Baseline AUC
Jan 1, 2017	85.5	81.9
July 1, 2017	84.0	82.0
Jan 1, 2018	83.9	81.2
July 1, 2018	83.8	81.2

embedding, self-attention mechanism and prediction head were also ablated. Our time embedding is shown to be as good as if not better than alternatives such as learning embeddings for each unique visit timestamp and allowing the vector ω of frequencies to be a learned parameter of the model. We likewise find that our convolutional prediction head gives performance increases versus a naive alternative that predicts directly from a sum of all contextualized visit embeddings.

Our ablation studies show that in addition to architectural innovations, reverse distillation is a key driver in SARD’s performance gains. Indeed, the smallest difference in ablated performance was observed when SARD’s self-attention architecture was replaced with a recurrent equivalent, but reverse distillation was still used for pretraining, indicating at reverse distillation’s universal applicability.

Model Transfer across Time. We consider how well a model trained on data from one time period transfers to the future. Our model for End of Life was trained on data from 2016 and earlier to predict deaths between April and September of 2017. The same model was then used to predict outcomes at various times in the future, as seen in Table 2. We find that performance does not degrade as we continue to apply it to data up to one year later, and that the model is still able to outperform linear baselines. We believe this is partly due to the normalization of data through the use of OMOP-standard codes and the well-regularized nature of our models.

5.2 Model Introspection

In healthcare applications, it is critical to understand and interpret how models make predictions. By developing the tools to do so, we also elucidate the method by which SARD is able to outperform baselines. We aim to deeply understand SARD by determining which visits are most influential in the prediction head and how those visits leverage self-attention to contextualize. We propose a local method for introspection to answer these questions on a per-prediction level, and use these techniques in Appendix Section 9 to interpret the case of a ≥ 90 year-old female patient who died between April and September of 2017. We find that SARD assigns a high probability (71.1%) of death for this patient on the prediction date of Jan 1, 2017, but that the linear model (5.4%) fails to do so.

To determine which visits are most influential to a prediction, we introspect directly on our convolutional prediction head. In notating this introspection, we suppress indices corresponding to batches (i.e. patients), as the introspection will be ultimately performed at the level of a single individual.

Recall that the prediction head convolves K kernels of size $d_e \times 1$ with the final contextualized visit representations, then uses a max-pooling operation to return the maximum cross-correlation between the kernel and any individual contextualized visit. Then, for the k^{th} of these K kernels, denote this maximum cross-correlation value by χ_k , and the maximizing visit by ν_i . Further, let w_k denote the weight given to the output from the k^{th} kernel in the final linear layer mapping to a prediction. We assign a score of $s(V_j) = \sum_k [[V_j = \nu_k]] w_k \sigma(\chi_k)$ to visit V_j , where σ represents the sigmoid nonlinearity applied after max-pooling. This metric represents the total importance of visit V_j by summing

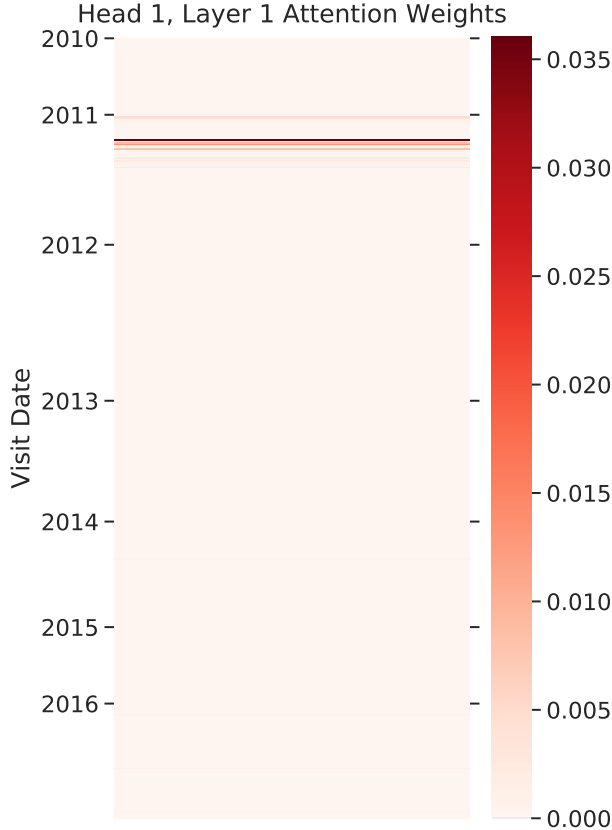


Figure 2: Attention weights for the case study patient’s top visit, from the first layer of the first head of the self-attention mechanism. While this top visit occurred in 2016, relatively close to the prediction date, it attends strongly to visits from 2011 indicating a serious episode of the same underlying atherosclerotic vascular disease present in the top visit, better contextualizing the patient’s risk. Similar images for other prediction heads and layers are displayed in Appendix Figure 5

all of its possible contributions to the final prediction. Using this metric, we can find the most predictive visits for our case study patient, and we present her top four visits in Appendix Table 4.

We also seek to understand how each visit is contextualized by examining its attention weights in SARD’s self-attention layers. For example, we examine the visits that the case study patient’s top visit attends to most strongly; we include these results in Appendix Table 5 and visualize a subset of the attention weights from her top visit in Figure 2. While this patient’s top visit occurred in 2016 and included detection of a myocardial infarction along with other cardiovascular disease, Figure 2 clearly shows that the top visit strongly attends to a cluster of visits in 2011.

By carefully analyzing these visits, we find that during the 2011 visits, the patient experienced other manifestations of atherosclerotic vascular disease. We conjecture that these continued, albeit more minor, cardiovascular issues over the years provide context for the 2016 visit, and ultimately augment the risk of death associated with the events of the 2016 visit. More generally, introspecting on the SARD model reveals that its self-attention mechanism leverages important contextual information from throughout a patient’s history to gain a nuanced understanding of which parts of the medical timeline are most important for prediction.

Thus, in addition to SARD’s quantitative gains, we also find that the deep model is able to make better predictions than simpler baselines when it is necessary to interpret an entire clinical narrative. In particular, in cases where SARD outperforms linear baselines, patients have significantly *more* data, as measured by the patient’s total number of visits, than in cases where the linear baseline outperforms (Mann-Whitney U test, $p < .05$).

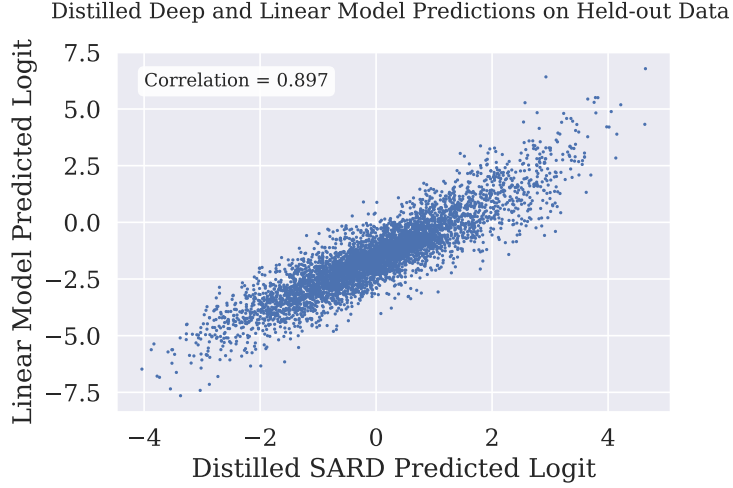


Figure 3: Comparison of Predictions on Held-out Data by Reverse Distilled and Linear Models

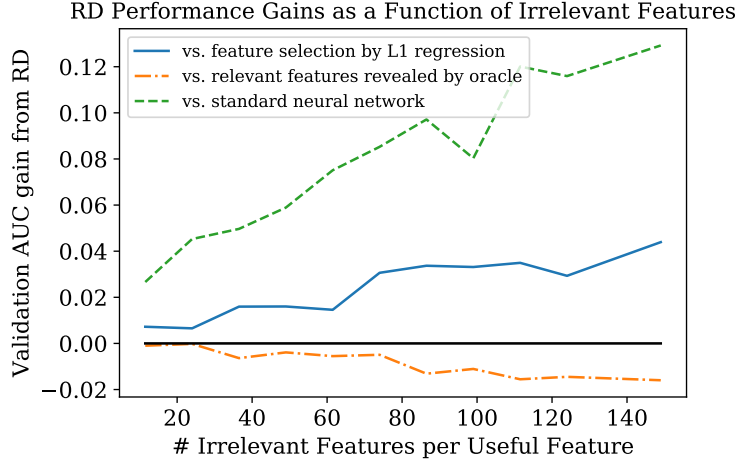


Figure 4: Reverse distillation AUC gains on synthetic data, as a function of sparsity of useful features

5.3 Analyses of Reverse Distillation.

We empirically validate that the SARD model for the End of Life task after reverse distillation (but before fine-tuning) generalizes in the same way as a linear model by analyzing the predictions made by both models on a held-out validation set. As seen in Figure 3, we find a Spearman correlation of 0.897 between the logit outputs of the two models on held-out data². This indicates that even for unseen patients, the models make similar predictions. Thus, the reverse-distilled deep model does indeed mimic the linear model, not just memorize its outputs at certain points.

Reverse distillation is further analyzed via experiments on synthetic data in Appendix Section 11. We find performance gains through reverse distillation for classification problems where data are poorly separated, or where only a small fraction of features are relevant, both properties of our prediction tasks. The ability of reverse distillation to enhance performance in synthetic scenarios with this property is shown in Figure 4, where we additionally compare to alternative feature-selection methods.

These experiments support that in addition to generalizing in the same way as an underlying linear model, a deep model trained via reverse distillation learns a soft version of the feature-selection performed by a regularized linear model. This is especially interesting in the case of multi-dimensional time-series data, where a simpler feature selection algorithm is not applicable. Indeed, in the case of longitudinal data, we would need to select a temporal context per

²Recall that the logit corresponding to an output probability p is $\log(p/(1-p))$

feature, not just the features themselves. A naive approach, such as limiting our SARD to the features selected by the windowed linear baseline for any time window, results in no performance gains versus the baseline for all three tasks.

6 Conclusions and Discussion of Model Impact

Fundamental advances in deep learning allow for large performance increases in many domains, but in healthcare, state-of-the-art models often still relied on rule-based heuristics and feature-engineering. We present a deep learning solution to the problem of making predictions using longitudinal health data: SARD, a self-attention based architecture that extracts contextual information across timelines of medical events. Significant performance gains using this model are underpinned by the use of reverse distillation, our novel pre-training procedure which demonstrably allows a deep model to be initialized to mimic a simpler but performant baseline. Using these innovations, we are able to exceed state-of-the-art performance for several medical prediction tasks. To our knowledge, SARD is the first successful adaptation of the self-attention paradigm to structured longitudinal health data.

Reverse distillation is just one successful method by which self-attention based predictive models can be initialized – in natural language processing, similar architectures have been found to substantially benefit from unsupervised learning with tasks such as imputing words or predicting sentence order [26]. Now that we have demonstrated that these architectures perform competitively on longitudinal clinical data, it opens the door to similarly designing unsupervised learning tasks to improve performance even further. Furthermore, while we are able to introspect and interpret predictions made by SARD at an individual level, future work may find more global ways to interpret how visits attend to each other through the lens of medical logic, similar to how self-attention as applied to natural language has been found to replicate nuanced grammatical and linguistic phenomena [32].

Machine learning as applied to healthcare has the potential to greatly improve outcomes for patients. Our work in particular has the primary application of being used to determine which patients would benefit from interventions, which could obviate the need for more intensive and invasive treatments in the future.

If implemented successfully, our model would have several positive impacts in healthcare. Our results also have the potential to impact the machine learning community:

- **Improved interventions** for patients. If we are able to correctly predict when patients will suffer adverse outcomes sufficiently far into the future, clinicians will be able to intervene to help prevent or ameliorate the impact of these potential issues.
- **The extension of self-attention to clinical machine learning**, which we believe is of great interest due to the potential for performance gains and increased interpretability. SARD’s success shows that such models can indeed work in practice, and can serve as a starting point for further research.
- **Combining expert domain knowledge and deep learning** through reverse distillation. Our new training method is a novel way to adapt and improve upon high-performing algorithms that rely on heuristics and data-engineering. This has the potential to inspire performance gains in healthcare, where such models are prevalent, but in other domains as well.

When work like ours is deployed in the field, it is critical to regularly determine how well the algorithms perform in general, how fairly they allocate resources, and how their predictions actually affect patient outcomes. The following considerations summarize some of the risks that must be mitigated when using SARD in a live clinical setting:

- **Equity of access** is a key goal in healthcare. Like many deep-learning paradigms, SARD performs better on some cases than others. For example, we find that it performs better on patients for whom more data is available. Such properties put groups of people for whom less data is available, or are otherwise disadvantaged in terms of model performance, at risk of less accurate predictions, and therefore less effective interventions [33]. Our future work will focus on analyzing SARD and its predictions as well as downstream pipelines that ingest these predictions from the perspective of algorithmic fairness [34]. This will help to ensure that SARD can indeed be used to help improve outcomes for all.
- **Clinical usage** of predictions from SARD should serve to actually improve patient outcomes. Even when predictions are accurate and fair, they also must be used appropriately to enhance care. Medical researchers have already set forth ethical and clinical guidelines governing how one should use predictions of sensitive events such as end of life [35], and in order for SARD’s performance to indeed translate to improved patient outcomes it is necessary that such principles are properly followed. Furthermore, the downstream application of SARD’s predictions must be considered *a priori* to determine how outcomes and cohorts are to be defined – the differentiation between an End of Life model which determines when to administer palliative care and one

which determines when to increase treatment to prolong life is a subtle example of how users of SARD must carefully appraise their medical objectives before developing tasks and deploying models.

Acknowledgements

This work was supported by Independence Blue Cross and would not have been possible without the advice and support of Aaron Smith-McLallen, Ravi Chawla, Kyle Armstrong, Luogang Wei, and Jim Denyer. The Tesla K80 GPUs used for this paper were donated by the NVIDIA Corporation.

References

- [1] Muhammad A Ahmad, Carly Eckert, Greg McKelvey, Kiyana Zolfagar, Anam Zahid, and Ankur Teredesai. Death vs. data science: predicting end of life. In *Thirty-Second AAAI Conference on Artificial Intelligence*, 2018.
- [2] Ashish Vaswani, Noam Shazeer, Niki Parmar, Jakob Uszkoreit, Llion Jones, Aidan N Gomez, Łukasz Kaiser, and Illia Polosukhin. Attention is all you need. In *Advances in neural information processing systems*, pages 5998–6008, 2017.
- [3] Alexandru Niculescu-Mizil and Rich Caruana. Predicting good probabilities with supervised learning. In *Proceedings of the 22nd international conference on Machine learning*, pages 625–632, 2005.
- [4] Narges Razavian, Jake Marcus, and David Sontag. Multi-task prediction of disease onsets from longitudinal laboratory tests. In *Machine Learning for Healthcare Conference*, pages 73–100, 2016.
- [5] Edward Choi, Mohammad Taha Bahadori, Le Song, Walter F Stewart, and Jimeng Sun. Gram: graph-based attention model for healthcare representation learning. In *Proceedings of the 23rd ACM SIGKDD International Conference on Knowledge Discovery and Data Mining*, pages 787–795, 2017.
- [6] Narges Razavian, Saul Blecker, Ann Marie Schmidt, Aaron Smith-McLallen, Somesh Nigam, and David Sontag. Population-level prediction of type 2 diabetes from claims data and analysis of risk factors. *Big Data*, 3(4):277–287, 2015.
- [7] Anand Avati, Kenneth Jung, Stephanie Harman, Lance Downing, Andrew Ng, and Nigam H Shah. Improving palliative care with deep learning. *BMC medical informatics and decision making*, 18(4):122, 2018.
- [8] Riccardo Miotto, Li Li, Brian A Kidd, and Joel T Dudley. Deep patient: an unsupervised representation to predict the future of patients from the electronic health records. *Scientific reports*, 6(1):1–10, 2016.
- [9] Alvin Rajkomar, Eyal Oren, Kai Chen, Andrew M Dai, Nissan Hajaj, Michaela Hardt, Peter J Liu, Xiaobing Liu, Jake Marcus, Mimi Sun, et al. Scalable and accurate deep learning with electronic health records. *NPJ Digital Medicine*, 1(1):18, 2018.
- [10] Manzil Zaheer, Satwik Kottur, Siamak Ravanbakhsh, Barnabas Poczos, Russ R Salakhutdinov, and Alexander J Smola. Deep sets. In *Advances in neural information processing systems*, pages 3391–3401, 2017.
- [11] Edward Choi, Mohammad Taha Bahadori, Andy Schuetz, Walter F Stewart, and Jimeng Sun. Doctor ai: Predicting clinical events via recurrent neural networks. In *Machine Learning for Healthcare Conference*, pages 301–318, 2016.
- [12] Edward Choi, Mohammad Taha Bahadori, Jimeng Sun, Joshua Kulas, Andy Schuetz, and Walter Stewart. Retain: An interpretable predictive model for healthcare using reverse time attention mechanism. In *Advances in Neural Information Processing Systems*, pages 3504–3512, 2016.
- [13] Rajesh Ranganath, Adler J Perotte, Noémie Elhadad, and David M Blei. The survival filter: Joint survival analysis with a latent time series. In *UAI*, pages 742–751, 2015.
- [14] Bum Chul Kwon, Min-Je Choi, Joanne Taery Kim, Edward Choi, Young Bin Kim, Soonwook Kwon, Jimeng Sun, and Jaegul Choo. Retainvis: Visual analytics with interpretable and interactive recurrent neural networks on electronic medical records. *IEEE transactions on visualization and computer graphics*, 25(1):299–309, 2018.
- [15] Zhengping Che, Sanjay Purushotham, Kyunghyun Cho, David Sontag, and Yan Liu. Recurrent neural networks for multivariate time series with missing values. *Scientific reports*, 8(1):1–12, 2018.
- [16] Ethan Steinberg, Ken Jung, Jason A Fries, Conor K Corbin, Stephen R Pfahl, and Nigam H Shah. Language models are an effective patient representation learning technique for electronic health record data. *arXiv preprint arXiv:2001.05295*, 2020.
- [17] Hrayr Harutyunyan, Hrant Khachatrian, David C Kale, Greg Ver Steeg, and Aram Galstyan. Multitask learning and benchmarking with clinical time series data. *Scientific data*, 6(1):1–18, 2019.

[18] Junyi Gao, Cao Xiao, Yasha Wang, Wen Tang, Lucas M Glass, and Jimeng Sun. Stagenet: Stage-aware neural networks for health risk prediction. In *Proceedings of The Web Conference 2020*, pages 530–540, 2020.

[19] Fenglong Ma, Yaqing Wang, Houping Xiao, Ye Yuan, Radha Chitta, Jing Zhou, and Jing Gao. A general framework for diagnosis prediction via incorporating medical code descriptions. In *2018 IEEE International Conference on Bioinformatics and Biomedicine (BIBM)*, pages 1070–1075. IEEE, 2018.

[20] Fan Zhang, Tong Wu, Yunlong Wang, Yong Cai, Cao Xiao, Emily Zhao, Lucas Glass, and Jimeng Sun. Predicting treatment initiation from clinical time series data via graph-augmented time-sensitive model. *arXiv preprint arXiv:1907.01099*, 2019.

[21] Fenglong Ma, Radha Chitta, Jing Zhou, Quanzeng You, Tong Sun, and Jing Gao. Dipole: Diagnosis prediction in healthcare via attention-based bidirectional recurrent neural networks. In *Proceedings of the 23rd ACM SIGKDD international conference on knowledge discovery and data mining*, pages 1903–1911, 2017.

[22] Liantao Ma, Chaohe Zhang, Yasha Wang, Wenjie Ruan, Jiangtao Wang, Wen Tang, Xinyu Ma, Xin Gao, and Junyi Gao. Concare: Personalized clinical feature embedding via capturing the healthcare context. In *Proceedings of the AAAI Conference on Artificial Intelligence*, volume 34, pages 833–840, 2020.

[23] Jacob Devlin, Ming-Wei Chang, Kenton Lee, and Kristina Toutanova. Bert: Pre-training of deep bidirectional transformers for language understanding. *arXiv preprint arXiv:1810.04805*, 2018.

[24] Neo Wu, Bradley Green, Xue Ben, and Shawn O’Banion. Deep transformer models for time series forecasting: The influenza prevalence case. *arXiv preprint arXiv:2001.08317*, 2020.

[25] Shiyang Li, Xiaoyong Jin, Yao Xuan, Xiyou Zhou, Wenhui Chen, Yu-Xiang Wang, and Xifeng Yan. Enhancing the locality and breaking the memory bottleneck of transformer on time series forecasting. In *Advances in Neural Information Processing Systems*, pages 5244–5254, 2019.

[26] Youngduck Choi, Chill Yi-I Chiu, and David Sontag. Learning low-dimensional representations of medical concepts. *AMIA Summits on Translational Science Proceedings*, 2016:41, 2016.

[27] Geoffrey Hinton, Oriol Vinyals, and Jeff Dean. Distilling the knowledge in a neural network. *arXiv preprint arXiv:1503.02531*, 2015.

[28] George Hripcsak, Jon D Duke, Nigam H Shah, Christian G Reich, Vojtech Huser, Martijn J Schuemie, Marc A Suchard, Rae Woong Park, Ian Chi Kei Wong, Peter R Rijnbeek, et al. Observational health data sciences and informatics (ohdsi): opportunities for observational researchers. *Studies in health technology and informatics*, 216:574, 2015.

[29] Adam Paszke, Sam Gross, Francisco Massa, Adam Lerer, James Bradbury, Gregory Chanan, Trevor Killeen, Zeming Lin, Natalia Gimelshein, Luca Antiga, Alban Desmaison, Andreas Kopf, Edward Yang, Zachary DeVito, Martin Raison, Alykhan Tejani, Sasank Chilamkurthy, Benoit Steiner, Lu Fang, Junjie Bai, and Soumith Chintala. Pytorch: An imperative style, high-performance deep learning library. In H. Wallach, H. Larochelle, A. Beygelzimer, F. d’Alché-Buc, E. Fox, and R. Garnett, editors, *Advances in Neural Information Processing Systems 32*, pages 8024–8035. Curran Associates, Inc., 2019.

[30] Diederik P Kingma and Jimmy Ba. Adam: A method for stochastic optimization. *arXiv preprint arXiv:1412.6980*, 2014.

[31] Elizabeth R DeLong, David M DeLong, and Daniel L Clarke-Pearson. Comparing the areas under two or more correlated receiver operating characteristic curves: a nonparametric approach. *Biometrics*, pages 837–845, 1988.

[32] Yongjie Lin, Yi Chern Tan, and Robert Frank. Open sesame: Getting inside bert’s linguistic knowledge. *arXiv preprint arXiv:1906.01698*, 2019.

[33] Ziad Obermeyer, Brian Powers, Christine Vogeli, and Sendhil Mullainathan. Dissecting racial bias in an algorithm used to manage the health of populations. *Science*, 366(6464):447–453, 2019.

[34] Irene Chen, Fredrik D Johansson, and David Sontag. Why is my classifier discriminatory? In *Advances in Neural Information Processing Systems*, pages 3539–3550, 2018.

[35] W Daniel Doty and Robert M Walker. Medical futility. *Clinical cardiology*, 23(S2):6–16, 2000.

[36] Craig A Martin, PL Thompson, BK Armstrong, MS Hobbs, and Nicholas de Klerk. Long-term prognosis after recovery from myocardial infarction: a nine year follow-up of the perth coronary register. *Circulation*, 68(5):961–969, 1983.

Appendices

7 Ablation Studies

In this appendix we complement our architecture design with an empirical evaluation of several ablation studies. Our objective here is to show that our design choices perform better than alternatives. As can be seen in Table 3, we find statistical and computational justifications for our architecture. As seen in Figure 1, the SARD architecture naturally splits into modular parts, the three most important of which we investigate via ablation.

7.1 Temporal Embedding

We utilized a fixed vector of frequencies to generate our sinusoidal time embeddings, in line with past work [2] in self-attention, which found that learned time embeddings were not significantly more performant. We confirm this by swapping out the fixed-frequency time embedding for several alternative options and confirming that performance does not increase. We define these alternatives as follows:

- Learned Sinusoidal Embeddings: we set $\tau(V_j^i) = \mathbf{a} \odot \sin(t_j^i \omega + \rho) || \mathbf{a} \odot \cos(t_j^i \omega + \rho)$, where \mathbf{a} is a learned vector of amplitudes, ω a learned vector of frequencies and ρ a learned vector of phases. Note that the operator \odot denotes element-wise multiplication. We find that this flexibility is not necessary to improve performance when compared to an embedding using a fixed choice of frequencies, unit amplitudes and zero phases.
- Learned Embeddings: We treat each unique value of t_j^i as an independent token, and embed this token using a trained embedding matrix.
- No Time Embeddings: We set $\tau(V_j^i) = 0$. The fact that performance does not completely degrade here indicates that a combination of non-temporal features and the relative ordering of visits is enough to achieve decent performance, but not as performant as fully incorporating temporal data.

Note that reverse distillation is used in all cases of temporal embedding ablation.

7.2 Self-attention

A novel aspect of our work is its use of a self-attention architecture as a tool to ingest time-series of embedded clinical data. In the past, RNN-based approaches [11, 12, 21] have been the state-of-the-art, and as such we developed an ablation study in which we replace our architecture with a unidirectional recurrent GRU-cell network, leaving the rest of the network unchanged. This GRU-cell network used input dimension $d_e = 300$ and hidden dimension $d_e = 300$.

In table 3, the row RNN (without RD) corresponds to this ablated model trained from a random initialization, and RNN + RD to the ablated model trained using the same reverse distillation procedure used in SARD + RD.

We performed a similar ablation in which we replaced the the self-attention layers with the identity, to further evaluate the value of explicitly contextualizing visits. In table 3, the row Identity (without RD) corresponds to this ablated model trained from a random initialization, and Identity + RD to this model trained using the same reverse distillation procedure used in SARD + RD.

To ensure that our ablation fairly compared recurrent and self-attention based approaches, we preserved all other architectural elements including the visit-level input embeddings, use of temporal embeddings (fixed-frequency sinusoidal time embeddings led to the best performance), and the prediction head to aggregate the final visit representations, which here operates on the hidden states of each element of the last layer of the RNN. We found the prediction head’s aggregation to be more performant and serve as a more apt comparison than the standard recurrent technique of simply predicting from the hidden state of the last element of the last layer of the RNN. This design choice helps mitigate the fact that older visits may be ‘forgotten’ by the RNN, by allowing these visits to directly influence the inputs of the prediction head. We find that the self-attention architecture is competitive with the RNN, so long as the RNN is also trained with reverse distillation. An important finding is that reverse distillation can also be used to successfully train highly-performant recurrent models, further validating the usefulness of this method and indicating that it can be used more generally.

7.3 Prediction Head

We finally ablate our prediction head by replacing it with a naive alternative which simply sums the contextualized vector representations of all visits to obtain a vector $\tilde{\psi}(V_j^i)$ representing the entire history of patient i . This summed

Table 3: Ablation Study Results. + RD indicates that reverse distillation is used for pretraining

Design Choice \ Task Name	EoL	Surgery	LoH
SARD + RD	85.5	83.6	74.6
SARD (without RD)	84.4	82.9	73.1
Learned Sinusoidal Embeddings	85.0	83.7	74.7
Learned Embeddings	85.7	83.3	74.6
No Time Embeddings	84.8	82.6	74.0
RNN + RD	86.0	83.0	74.7
RNN (without RD)	84.9	82.5	72.9
Identity + RD	85.2	82.2	74.3
Identity (without RD)	84.8	81.8	73.3
Summing Head + RD	85.1	83.1	73.9
Summing Head (without RD)	83.0	81.8	72.1

vector, which will have dimension d_e , is then passed into a single linear layer with sigmoid activation to make a final prediction. We use input embedding, sinusoidal time embedding and a self attention mechanisms identical to those of the SARD model described in Section 3.

We find that SARD’s convolutional prediction head gives performance increases when compared with this simpler alternative. Even in this regime, we again find that reverse distillation allows models to be more performant. In table 3, the row Summing Head (without RD) corresponds to this ablated model trained from a random initialization, and Summing Head + RD to this model trained using the same reverse distillation procedure used in SARD + RD.

8 Proof Sketch of Lemma 1

We show that a single self-attention head can generate the vector $f_i(W)$, of size $|f_i(W)|$, for a given window $[T_A - T, T_A]$ as described in section 4, thus implying that several self-attention heads’ concatenated output can generate the concatenation of several $f_i(W)$ vectors.

Set the embedding function $\phi(c)$ to simply return a one-hot encoding of the code c , concatenated with d_e zeros. We further set g to be an identity function. Then for all i, j , $\psi(V_j^i)$ will be a multi-hot binary vector whose nonzero elements correspond to the codes in C_j^i .

We note that our time embedding per visit will be $\tau(V_j^i) = \sin(t_j^i \omega) \parallel \cos(t_j^i \omega)$. We set the first $|\mathcal{C}|$ elements of ω to zero, so that visit embedding $\psi(V_j^i) + \tau(V_j^i)$ will be fully separable component-wise into a multi-hot vector of codes and a time embedding.

The self-attention mechanism will use a linear map from $\psi(V_j^i) + \tau(V_j^i)$ to three vectors k_j^i, q_j^i, v_j^i called the key, query and value vectors respectively, and create the contextual embedding $\sum_{j'=1}^{n_v} (q_j^i \cdot k_{j'}^i) v_{j'}^i$ for visit V_j^i . We allow v_j^i to simply be the multi-hot encoding $\psi(V_j^i)$. Note that since $\psi(V_j^i)$ and $\tau(V_j^i)$ have different nonzero components that this can be achieved by a simple matrix multiplication from $\psi(V_j^i) + \tau(V_j^i)$.

Next, we create appropriate length-1 key and query vectors. We define $k_j^i = q_j^i = [[t_j^i < T]]$, and under this definition the contextual embedding of every visit V_j^i where $t_j^i < T$ will become $\sum_{j'=1}^{n_v} [[t_{j'}^i < T]] v_{j'}^i$, which is a multi-hot vector whose nonzero entities correspond to all codes seen in the window of the past T days.

It remains to show how we would construct $k_j^i = q_j^i = [[t_j^i < T]]$ as a linear transformation of $\psi(V_j^i) + \tau(V_j^i)$. We do so by invoking a Fourier analysis argument. Let P be the length of the interval from the first event in the dataset to T_A . Then, $[[t_j^i < T]]$ can simply be represented as a function of period P with value 1 in $[0, T]$ and 0 in $[T, P]$, which in turn can be represented as a Fourier series with coefficient $\frac{2}{n\pi} \sin^2(\frac{n\pi T}{P})$ corresponding to $\sin(\frac{2n\pi t}{P})$ and coefficient $\frac{1}{n\pi} \sin(\frac{n\pi T}{P})$ corresponding to $\cos(\frac{2n\pi t}{P})$. Thus, for appropriately chosen ω that includes values of the form $2n\pi/P$, we can recover an arbitrarily good approximation of $[[t_j^i < T]]$, thus allowing us to use a single self-attention head to mimic a single windowed feature vector as passed into the linear model. The convolutional prediction head can simply apply an identity transformation by setting each of $|f_i(W)|$ kernels equal to the vectors of the standard basis for $\mathbb{R}^{|f_i(W)|}$ – after the max pooling operation filters corresponding to nonzero elements of $f_i(W)$ will return a one, and

those corresponding to elements of $f_i(W)$ will return a 0, effectively implementing the identity transformation on this binary vector.

Using multiple self-attention heads, we can obtain the concatenation of several windowed feature vectors, and passing these through the prediction head allows us to fully replicate the functionality of the linear model using the deep model.

9 SARD Extracted Timeline Case Study

In this appendix we qualitatively investigate the ability of SARD to generalize and contextualize better than a linear model through a case study.

In order to convert the soft predictions of SARD and our baseline windowed linear model to binarized predictions of outcomes, we chose decision thresholds for both models to ensure a false positive rate of 0.25 on a validation set – this resulted in thresholds of 0.34 and 0.33 for SARD and the linear model respectively. We note that in practice the selection of a threshold, or alternatively the use of these scores as rankings, would be driven by varied downstream applications.

We consider a female patient who died between April and September of 2017 (she was ≥ 90 years old at the time), an event that was correctly predicted by SARD (probability of 71.1%) but not by our linear baseline (probability of 5.4%). She had an active medical history, with over 700 recorded medical visits. To better understand why SARD accurately predicts her death while logistic regression does not, we introspect on which visits are most influential in the prediction head of the model, and how those visits were benefited by the self-attention architecture.

To determine which visits were most influential in the prediction made by SARD, we use the score $s(V_j) = \sum_k [[V_j = \nu_k]] w_k \sigma(\chi_k)$ to assign an importance to visit V_j , as defined in Section 5.2.

The specific visit that maximizes the above score, which we denote as the *top visit*, occurred in 2016, a few months before the patient’s death. During this visit, she was treated for a chronic ulcer of skin of lower leg, with both anesthesia procedure(s) and Debridement, muscle and/or fascia procedures performed. The visit also notes that the patient experienced atrial fibrillation, Pure hypercholesterolemia, Non-rheumatic aortic sclerosis, and hypothyroidism, and that an old myocardial infarction was detected. Further details of this visit are provided in Table 4.

While some of the codes in this visit, such as the treatment of an ulcer, are not immediately alarming in their own right and are therefore not highly weighted by the linear model, this patient’s history of ongoing cardiovascular disease suggest that these conditions may indeed be manifestations of more serious underlying pathology. Aligning with medical intuition that the long-term survival rate of patients who suffer a myocardial infarction is highly dependent upon other risk factors [36], the linear model’s top weighted negative features are *Insertion and placement of flow directed catheter (Swan-Ganz)*, a procedure used diagnostically to determine and eliminate risks after a myocardial infarction, and *carvedilol*, a drug known to reduce risk of death after myocardial infarction, both over length- ∞ windows.

The SARD model, by contrast, is able to leverage important contextual information from throughout the patient’s history thanks to its self-attention mechanism. While the top visit occurred in 2016, SARD is able to build an understanding that the patient was at high cardiovascular risk at the time of prediction by strongly attending to visits encoding severe cardiovascular illness in 2011, as visualized in Figure 5. Indeed, all of the visits strongly attended to by the first layer of the first self-attention head of SARD for this patient are related to this 2011 episode, as seen in Table 5. These persistent and recent manifestations of the patient’s underlying cardiovascular disease provide context for more recent visits, and augment the relevance of cardiovascular disease at prediction time.

10 Training Details and Hyperparameter Choices

We display possible hyperparameter values for both our linear and SARD models in Table 6. These values were chosen using a validation set of 5000 patients.

As our models were trained on a small cluster of 4 GPUs, and our inputs were very high dimensional with around 1.9×10^6 features per person, it was critical for speed and feasibility to ingest data in a way that respected sparsity. As such, we made extensive use of *scatter* operations to aggregate visits together. We note that this allows us to perform initial embeddings of concepts and times using a single large tensor in GPU memory, then summing up relevant terms for each visit.

Table 4: The 4 most predictive visits for the case study patient, ranked by the score $s(V_j)$ developed in Section 5.2. While our models use specific visit dates, we only include visit year to censor protected health information (PHI).

Visit Importance Score: 0.487	
Year of Visit: 2016	
Codes:	
<ul style="list-style-type: none"> • Hypothyroidism • Calcium Chloride 0.0014 MEQ/ML / Potassium Chloride 0.004 MEQ/ML / Sodium Chloride 0.103 MEQ/ML / Sodium Lactate 0.028 MEQ/ML Injectable Solution • Anesthesia for procedures on the integumentary system on the extremities, anterior trunk and perineum; not otherwise specified • Unlisted anesthesia procedure(s) • Debridement, muscle and/or fascia (includes epidermis, dermis, and subcutaneous tissue, if performed); first 20 sq cm or less • Atrial fibrillation • Old myocardial infarction • 2 ML Fentanyl 0.05 MG/ML Injection • General Surgery 	<ul style="list-style-type: none"> • Anesthesiology • 20 ML Propofol 10 MG/ML Injection • Debridement, muscle and/or fascia (includes epidermis, dermis, and subcutaneous tissue, if performed); each additional 20 sq cm, or part thereof (List separately in addition to code for primary procedure) • Non-rheumatic aortic sclerosis • Chronic ulcer of foot • Pure hypercholesterolemia • Necrosis of ankle muscle co-occurrent and due to chronic ulcer of ankle • Chronic ulcer of skin of lower leg • Cefazolin 1000 MG Injection • Osteoporosis
Visit Importance Score: 0.467	
Year of Visit: 2015	
Codes:	
<ul style="list-style-type: none"> • Hypothyroidism • Collection of venous blood by venipuncture • Immunization administration (includes percutaneous, intradermal, subcutaneous, or intramuscular injections); 1 vaccine (single or combination vaccine/toxoid) • Office or other outpatient visit for the evaluation and management of an established patient, which requires at least 2 of these 3 key components: A detailed history; A detailed examination; Medical decision making of moderate complexity. Counseling and/o • Essential hypertension 	<ul style="list-style-type: none"> • Cardiology • Clinical Laboratory • 0.5 ML influenza B virus vaccine B/Brisbane/60/2008 antigen 0.12 MG/ML / Influenza Virus Vaccine, Inactivated A-California-07-2009 X-179A (H1N1) strain 0.12 MG/ML / Influenza Virus Vaccine, Inactivated A-Victoria-210-2009 X-187 (H3N2) (A-Perth-16-2009) st • Paroxysmal atrial fibrillation • Iron deficiency anemia • Pure hypercholesterolemia
Visit Importance Score: 0.345	
Year of Visit: 2016	
Codes:	
<ul style="list-style-type: none"> • 10 ML Nitroglycerin 5 MG/ML Injection • Ulcer of lower extremity • Anesthesia for diagnostic arteriography/venography • Unlisted anesthesia procedure(s) • Aortography, abdominal, by serialography, radiological supervision and interpretation • Angiography, extremity, bilateral, radiological supervision and interpretation • Anesthesia for patient of extreme age, younger than 1 year and older than 70 (List separately in addition to code for primary anesthesia procedure) 	<ul style="list-style-type: none"> • 5 ML Fentanyl 0.05 MG/ML Injection • Anesthesiology • Vascular Surgery • Lidocaine Hydrochloride 10 MG/ML Injectable Solution • Revascularization, endovascular, open or percutaneous, femoral, popliteal artery(s), unilateral; with transluminal angioplasty • Chronic atrial fibrillation • heparin sodium, porcine 1000 UNT/ML Injectable Solution • Atherosclerosis of native arteries of the extremities • Cefazolin 1000 MG Injection
Visit Importance Score: 0.337	
Year of Visit: 2011	
Codes:	
<ul style="list-style-type: none"> • Acquired hypothyroidism • Neurogenic bladder • Peptic ulcer without hemorrhage, without perforation AND without obstruction • Radiologic examination, chest; single view, frontal • Initial hospital care, per day, for the evaluation and management of a patient, which requires these 3 key components: A comprehensive history; A comprehensive examination; and Medical decision making of high complexity ... • Inpatient consultation for a new or established patient, which requires these 3 key components: A comprehensive history; A comprehensive examination; and Medical decision making of high complexity ... • Emergency department visit for the evaluation and management of a patient, which requires these 3 key components within the constraints imposed by the urgency of the patient's clinical condition and/or mental status: ... • Dyspnea • Atrial fibrillation 	<ul style="list-style-type: none"> • Aortic valve disorder • Heart murmur • Low blood pressure • Hypertensive heart disease without congestive heart failure • Coronary atherosclerosis • Disorder of kidney and/or ureter • Ankle ulcer • Coronary arteriosclerosis in native artery • Dizziness and giddiness • Acute myocardial infarction of anterior wall • Leukocytosis • Tachycardia • Chest pain • Osteoporosis

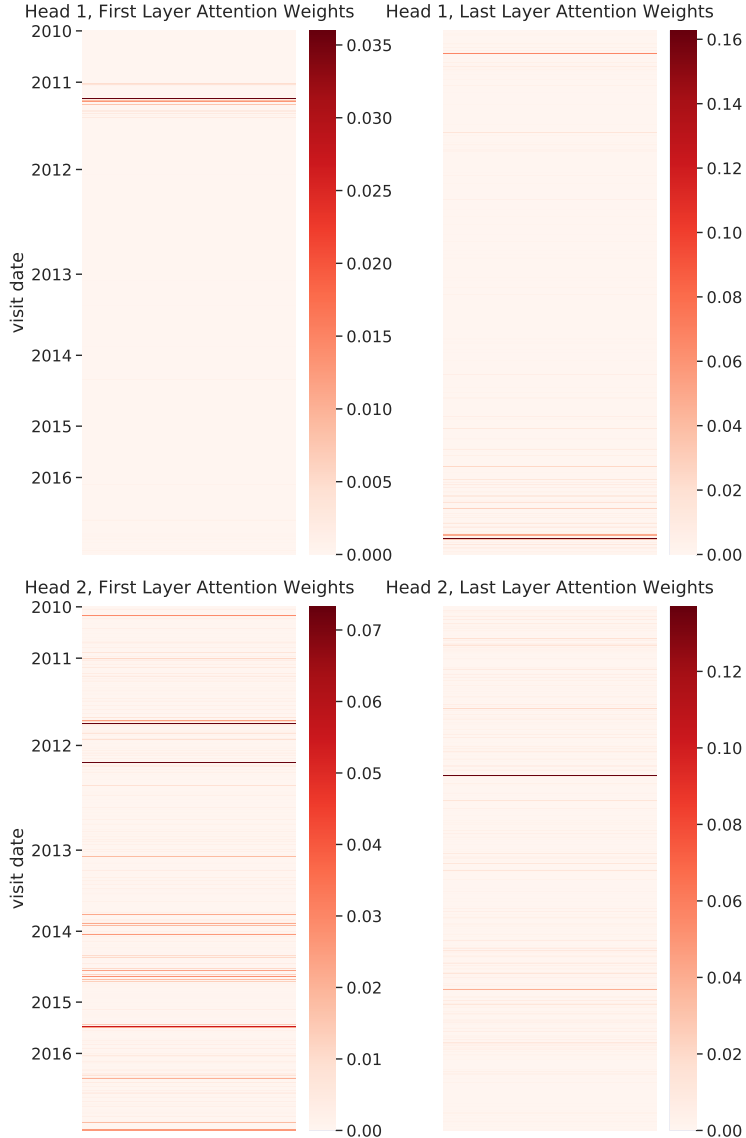


Figure 5: Attention weights for the case study patient’s ‘top visit.’ While the top visit occurred in 2016, it pulls context from visits throughout the patient’s history. Each panel contains a row for each of the patient’s 512 visits, colored by how much attention it is given by the top visit. Notably, the visits most highly attended to in the first layer of the first self-attention head (top left panel) represent a serious prior manifestation of the same underlying atherosclerotic vascular disease present in the top visit.

In addition, we accumulate gradients over multiple mini-batches to achieve a batch size of 500. Indeed, the largest batch size we are able to operate with varied from 20 to 50 depending on the model in question.

11 Reverse Distillation on Synthetic Data

It is not immediately obvious why reverse distillation helps model performance when utilized as a pre-training procedure. To help further empirically justify when and how reverse distillation works, we turn to experiments with synthetic data designed to mimic the distinct properties of the kind of data found in electronic health records. In particular, we are interested in data where:

- The data is high-dimensional but only a small fraction of these features are useful for any specific downstream task.

Table 5: The four visits most highly attended by the top visit from 2016; first layer, first self-attention head. We only include visit year in the table so as not to reveal PHI.

Attention from Top Visit: 0.0360

Year of Visit: 2011

Codes:

- Disorder of cardiovascular system
- Echocardiography, transthoracic, real-time with image documentation (2D), includes M-mode recording, when performed, complete, with spectral Doppler echocardiography, and with color flow Doppler echocardiography
- Duplex scan of extracranial arteries; complete bilateral study
- Subsequent hospital care, per day, for the evaluation and management of a patient, which requires at least 2 of these 3 key components: An expanded problem focused interval history; An expanded problem focused examination ...
- Acute myocardial infarction
- Angina pectoris

Attention from Top Visit: 0.0130

Year of Visit: 2011

Codes:

- Radiologic examination, chest; single view, frontal
- Atelectasis
- Aortic valve disorder

Attention from Top Visit: 0.0086

Year of Visit: 2011

Codes:

- Open and other replacement of aortic valve with tissue graft
- Anesthesia for direct coronary artery bypass grafting; with pump oxygenator
- Replacement, aortic valve, open, with cardiopulmonary bypass; with prosthetic valve other than homograft or stentless valve
- Arterial catheterization or cannulation for sampling, monitoring or transfusion (separate procedure); percutaneous
- Radiologic examination, chest; single view, frontal
- Level IV - Surgical pathology, gross and microscopic examination Abortion - spontaneous/missed Artery, biopsy Bone marrow, biopsy Bone exostosis Brain/meninges, other than for tumor resection Breast, biopsy, not requiring microscopic evaluation of surgical
- Decalcification procedure (List separately in addition to code for surgical pathology examination)
- Insertion and placement of flow directed catheter (eg, Swan-Ganz) for monitoring purposes
- Anesthesia for patient of extreme age, younger than 1 year and older than 70 (List separately in addition to code for primary anesthesia procedure)
- Atrial fibrillation
- Aortic valve disorder
- Essential hypertension
- Coronary atherosclerosis
- Operative external blood circulation
- Packed blood cell transfusion
- Echocardiography
- Chest pain

Attention from Top Visit: 0.0078

Year of Visit: 2011

Codes:

- Subsequent hospital care, per day, for the evaluation and management of a patient, which requires at least 2 of these 3 key components: An expanded problem focused interval history; An expanded problem focused examination ...
- Acute myocardial infarction

Table 6: Hyperparameters

Hyperparameter	Possible Values
λ	{0.05, 0.5, 5, 50}
\mathcal{W}_c	$[T_A - t', T_A]$ for all $t' \in \{15, 30, 60, 90, 180, 360, 540, 720, \infty\}$ days
α	{0, 0.05, 0.1, 0.15}

- The data is not fully separable, even in the limit of infinite data.

With these two properties in mind, synthetic data for a binary classification problem is generated as follows:

- First, two centers c_0, c_1 are chosen in \mathbb{R}^d , with a separation of $\|c_0 - c_1\| = \gamma$. We shift the clusters so that the origin is exactly between the two centers.
- Next, for each of N training points:
 - We draw a label y for the point from a Bernoulli distribution with parameter ρ .
 - We associate K features with the point. The first βK are drawn as iid Gaussian RVs with mean c_y and unit variance. The remainder are uninformative features drawn as iid Gaussians with mean 0 and unit variance.

We can manipulate the fraction of useful features and the separability of the classes by varying β and γ respectively. Our experiments are designed to find when reverse distillation is successful in excess of a simple feature selection procedure – the hypothesis is that reverse distillation would put weight on features similar to those chosen by the underlying linear model, but in a ‘soft’ and more robust way. As such, the baseline we choose to compare to is a deep model trained only on the features that are not zeroed out by a L_1 -regularized linear model.

We note that other, more complex feature selection baselines are possibilities. However, feature-selection in general is straightforward to implement in this synthetic model – one can simply slice out the features chosen by a procedure. With longitudinal medical data, we are not just selecting features temporal contexts as well, and it is not possible to iterate over all such selections. As such, reverse lets us do a “soft” feature selection over a very complex space of time-series features.

Concretely, we define four procedures whose performance we compare:

- Reverse Distill: We first train an L_1 -regularized logistic regression on a synthetic binary classification dataset, tuning the regularization with a validation set to maximize AUC. We collect the predictions $p_{LR}(x)$ made by the linear model at each training point x . Next, a multi-layer perceptron (MLP) with two densely connected layers with ReLU activation, followed by a sum and sigmoid activation to return a probability is initialized randomly and trained until convergence to minimize the KL-divergence between its predictions $MLP(x)$ and $p_{LR}(x)$. Finally, this MLP is fine-tuned by minimizing the loss

$$\ell(x, y) = \text{xent}(MLP(x), y) + \alpha D_{\text{KL}}(p_{LR}(x) \| MLP(x))$$

where α is a hyperparameter tuned on a validation set. Note that xent denotes the standard binary cross-entropy loss, weighted to account for class imbalance.

- Standard Neural Network: We create an MLP using the same architecture as Reverse Distill, and train it until convergence to minimize the loss $\ell(x, y) = \text{xent}(MLP(x), y)$.
- Feature Selection by L_1 regression: We first train an L_1 -regularized logistic regression as in Reverse Distill. Denote the weights of this model by w_i – we define a feature selection function $f_R(x) = \langle x_i \rangle_{\{i|w_i \neq 0\}}$ which takes a feature vector x and creates a new vector whose components correspond to the elements of x which would not be zeroes out by the regularized logistic regression. We create an MLP using the same architecture as Reverse Distill, and train it until convergence to minimize the loss $\ell(x, y) = \text{xent}(MLP(f_R(x)), y)$
- Feature Selection by Oracle: We define a feature selection function $f_O(x) = \langle x_i \rangle_{\{i|\text{feature } i \text{ is relevant}\}}$ which takes a feature vector x and creates a new vector whose components correspond to the βK elements of x which are actually relevant for prediction. We create an MLP using the same architecture as Reverse Distill, and train it until convergence to minimize the loss $\ell(x, y) = \text{xent}(MLP(f_O(x)), y)$. This model reflects an optimal feature selection procedure only possible with full knowledge of the generative process for the data, and should beat all other baselines.

We compare the differences in median AUCs on out-of-sample data between Reverse Distill and the other three models to investigate when reverse distillation is useful. Unless explicitly varied, we hold the data generation parameters at $K = 200, \gamma = 0.5, \rho = 0.05, \beta = 0.02$:

- We first investigate how the separability of the data affects the performance gains of reverse distillation by varying γ . We expect that at extremely low separability, no model will be able to do well, and at high separability all models will do equally well. Between these two extremes, we expect reverse distillation to outperform baselines. This is confirmed by our experimental results, as visualized in Figure 6
- We next investigate how the sparsity of useful features affects the performance gains of reverse distillation by varying α . We expect that as α decreases and we see less useful features, that reverse distillation will be more useful since it can make nuanced soft feature selections that can greatly help downstream performance. This is confirmed by our experimental results, as visualized in Figure 7
- We finally find that reverse distillation benefits from having more training data, which agrees with the intuition that a deeper, more nonlinear model will have a worse sample complexity. That being said, when an abundance of data is available reverse distillation is able to increase its edge over a baseline feature selection method. This is verified by our experimental results shown in Figure 8

12 Cohort Inclusion Criteria and Additional Dataset Details

In order to ensure that patients in our dataset had sufficient medical records to learn from, we created a *cohort* of patients whose medical history was sufficiently detailed for us to feel confident in making a data-driven prediction. Our

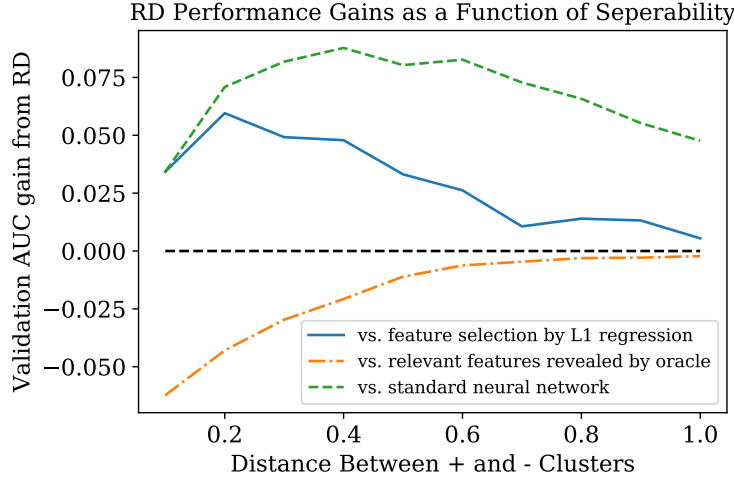


Figure 6: Reverse Distillation performance gains as a function of class separability

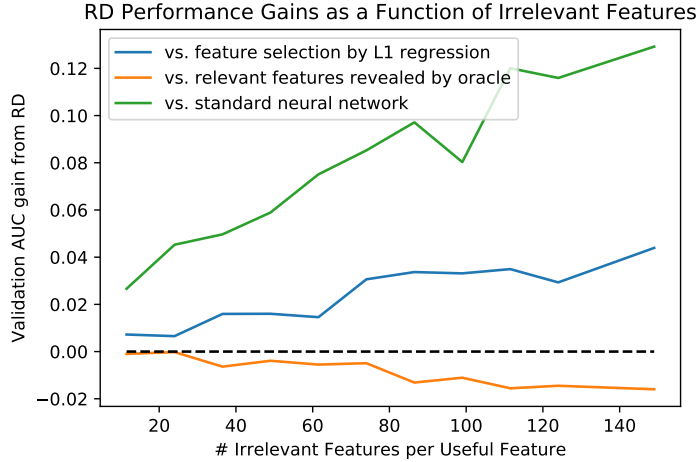


Figure 7: Reverse Distillation performance gains as a function of sparsity of useful features

inclusion criterion was that patients are enrolled in a Medicare insurance plan for all of the days in the one-year period leading up to the prediction date. For de-identification purposes, all patients whose age is over 90 have their age set to 90.

We split the 121,593 patients who satisfy these criteria into training, validation, and test sets of size 97,274, 5,000, and 19,319 respectively. Data was collected up to the end of the calendar year 2016, and outcomes measured between April and September 2017. We denote the set of all OMOP concepts used in the dataset by \mathcal{C} , which in our case is of size $|\mathcal{C}| = 37,004$. These codes include the drugs and procedures administered to the patient, the diagnosis codes recorded to justify these administrations, and the types of medical specialists with whom the patient interacted. The number of unique observed codes of each type in our feature set is shown in Figure 11, indicating the rich diversity of medical information that we can utilize in our models.

We receive varying amounts of data per patient, and note that the amount of data a patient has is in itself an interesting indicator of health; for example, a patient with a long medical history with very few visits may be inferred to be in better health, as they require less medical attention. We quantify the distributions characterizing the amount of information we have per patient in Figures 9 and 10. As shown in Figure 9, the length of a patient’s history, as measured from the time of their enrollment into an insurance plan tracked by our dataset to prediction time, ranges from 1 to 11 years, with a mean of 7.4 years – the minimum of one year results from the explicit exclusion of patients who entered a tracked insurance plan within one year of the prediction date. Additionally, as shown in Figure 10, the number of visits, or

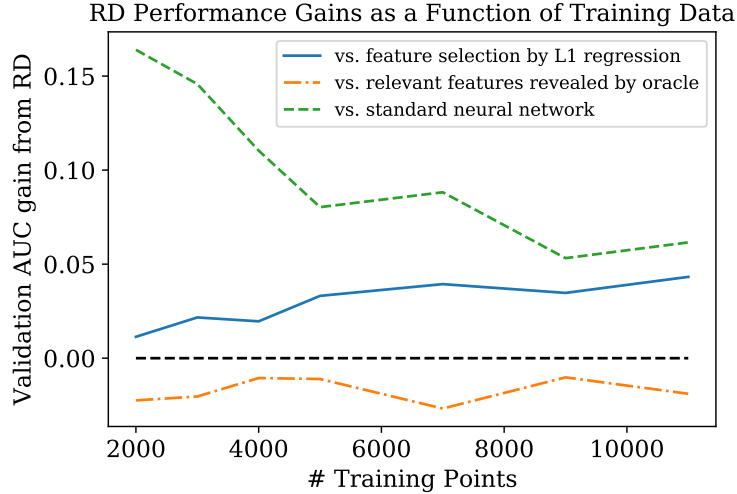


Figure 8: Reverse Distillation performance gains as a function of amount of training data

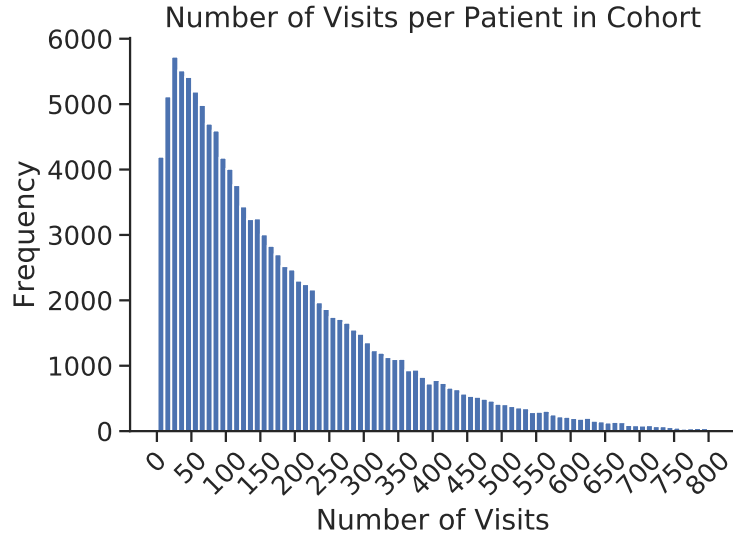


Figure 9: Histogram of the number of visits per patient. We clip the histogram at 800 visits, though a small subset of patients (0.4%) have more visits. Histogram buckets have a width of 10 visits.

unique days during which an interaction with the healthcare system took place, ranges from 1 to 1,616 per patient with a mean of 175. We note that after embedding visits, we truncate a patient’s history to include only her 512 most recent visits. This is done for computational efficiency purposes; even after this truncation, 95.78% of patients have their complete medical history included in the dataset.

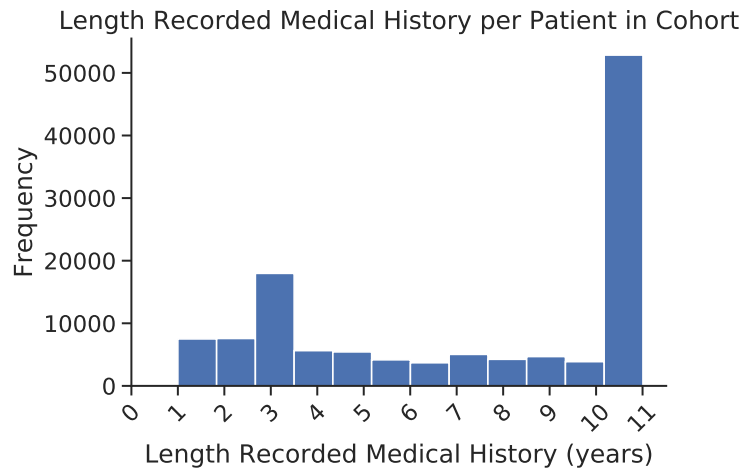


Figure 10: Histogram of recorded medical history length per patient.

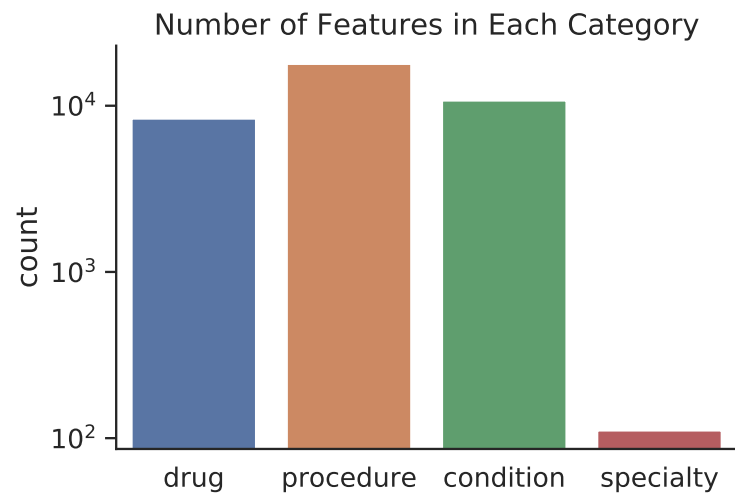


Figure 11: Breakdown of the 37,004 features in our dataset into their umbrella categories: drug administered, procedure performed, condition recorded, or specialty encountered. During a given visit, a patient will have features present from one or more of these categories.